

Control of a Transtibial Prosthesis with Monoarticular and Biarticular Actuators^{*}

Julian Zeiss^{*} Florian Weigand^{*} Martin Grimmer^{**}
Ulrich Konigorski^{*}

^{*} *Control Systems and Mechatronics Laboratory, Technical University of Darmstadt, Darmstadt, Germany, (e-mail: jzeiss@iat.tu-darmstadt.de)*

^{**} *Locomotion Laboratory, Institute of Sport Science, Technical University of Darmstadt, Darmstadt, Germany, (e-mail: grimmer@sport.tu-darmstadt.de)*

Abstract: Common active ankle joint prostheses comprise monoarticular actuators mimicking the function of the human soleus and tibialis anterior muscles, but lack the function of the biarticular human gastrocnemius muscle. Although these devices can mimic human ankle biomechanics in the sagittal plane, persons with transtibial amputation still show compensatory movements and asymmetric gait patterns. The goal of our research is to investigate the benefits of a biarticular transtibial prosthesis comprising mono- and biarticular actuators. This contribution presents the hardware configuration, control design and bypass testing of a biarticular prosthesis prototype with two actuators. A control structure consisting of a model-based feedforward control and a feedback controller to control the actuator torque is introduced. Modeling of the actuators and identification of all relevant system parameters is demonstrated. A reference trajectory based on healthy human ankle biomechanics and a control allocation are introduced. The system's capability to track desired torques is demonstrated in a walking experiment. It is able to generate human ankle torques and ankle angles with a variable distribution of torque between the mono- and biarticular actuator. Based on these results, further investigations on the torque allocation to improve the gait patterns of persons with transtibial amputation can be conducted.

Keywords: Active Prosthesis, Biarticular, Monoarticular, Transtibial, Torque Control, Series Elastic Actuators, Exoskeleton, Model-Based Feedforward Control

1. INTRODUCTION

Today's standard for persons with transtibial amputation (TTA) are passive energy storing and returning carbon fiber feet. They are designed to enable standing and locomotion, but lack the full range of motion (RoM) and power output of their human counterpart (Grimmer and Seyfarth (2014)). In recent years several active prostheses for the ankle joint such as BIOM (Herr and Grabowski (2011)) or Walk Run Ankle (WRA, Grimmer et al. (2017)) were developed. Although these active devices are capable of mimicking healthy human ankle kinematics and kinetics in the sagittal plane during level walking, asymmetries and compensatory strategies between impaired and unimpaired leg remain (Ferris et al. (2012)).

In particular, impaired legs show decreased knee RoM and knee flexion torque in terminal stance (Ferris et al. (2012)), which might be explained by the monoarticular actuation of the prosthetic devices. They only actuate the ankle joint and therefore only emulate the function of the monoarticular soleus and tibialis anterior muscles. The functionality

of the biarticular gastrocnemius muscle, which actuates the knee and the ankle joint simultaneously, is missing as a coupling between the impaired leg and the prosthesis.

Compared to monoarticular muscles, biarticular muscles have a range of different functionalities such as the transmission of forces between neighboring joints, the transfer of energy from powerful proximal to distal muscles and vice versa, and the synchronization and coordination of locomotor subfunctions (Schumacher et al. (2020)).

Several research groups have designed prosthetic prototypes to replicate the function of human gastrocnemius muscle in walking. Endo et al. (2009) used a quasi-passive clutched spring at the knee joint and an active ankle prosthesis. Eilenberg et al. (2018) combined an active knee orthosis and an active ankle prosthesis. Both designs emulate the function of the biarticular gastrocnemius muscle through the addition of a uniarticular actuator at the knee. Willson et al. (2020) presented a design physically connecting the thigh and the heel through a quasi-passive clutched spring. For all we know, so far there is no active prosthesis physically implementing an active actuation, that simultaneously actuates the knee and the ankle joint comparable to the human gastrocnemius muscle.

^{*} The authors gratefully thank the German Research Foundation (DFG) for funding this work by the project with the reference number KO 1876/15-1 and GR 4689/3-1.

A common approach for prosthetic and orthotic prototypes is the use of offboard actuators and power supply, reducing the masses worn by the user. Typically Bowden cables are used to apply forces on a worn device such as soft exosuits (Quinlivan et al. (2017)), ankle exoskeletons (Witte et al. (2015)) or knee orthoses (Eilenberg et al. (2018)).

Furthermore, the use of torque controlled series elastic actuators (SEAs) is common in the field of prostheses and orthoses. Typical control approaches for force control of series elastic actuators can be divided into two groups. The first transfers the force control problem into a position control problem (e.g. Kong et al. (2009); Grün et al. (2012)) by controlling the spring deflection and estimating the force from Hooke's law. This approach is suitable if the hardware setup contains a dedicated spring with known spring stiffness. The second group feeds back forces measured from force transducers, not relying on a specified elastic element and load position measurement. Subsets of PID control (e.g. Pratt and Williamson (1995)) or cascaded controllers with inner velocity and outer force loop (e.g. Vallery et al. (2007)) are used. In both cases feedforward terms are used to compensate actuator inertia and friction.

The goal of our research is to investigate the benefits of a prosthesis with mono- and biarticular actuation. We assume that such a prosthesis can improve the gait patterns of persons with TTA, compared to a prosthesis with monoarticular actuation only.

Therefore, this paper aims to introduce a hardware setup and a control structure, which enable the investigation of possible benefits of the additional biarticular actuation. The controlled system should be capable of generating human ankle torques and angles with a variable distribution of torque between mono- and biarticular actuator under laboratory conditions. Our future work will focus on how to split these torques between the mono- and biarticular actuators to improve the gait patterns of persons with TTA.

In this paper we describe the design and control of a biarticular prosthesis prototype, which extends an active ankle joint prosthesis with an additional biarticular actuator mimicking human gastrocnemius muscle function. To the best of our knowledge, this is the first prototype mechanically implementing an active gastrocnemius like actuator.

Through the outline of this paper we will present the hardware setup in Sec. 2. The modeling of both actuators and the identification of the system parameters is demonstrated in Sec. 3. Despite the differences between the actuators, a unified control scheme composed of a model-based feedforward control and a feedback controller will be used to control the torque of the ankle joint prosthesis and the force of the Bowden cable actuator in Sec. 4. Finally the system's capability of mimicking human ankle biomechanics including the gastrocnemius muscle function will be demonstrated in a walking experiment (Sec. 5). In a discussion (Sec. 6) and conclusion (Sec. 7) we will summarize the results of this work.

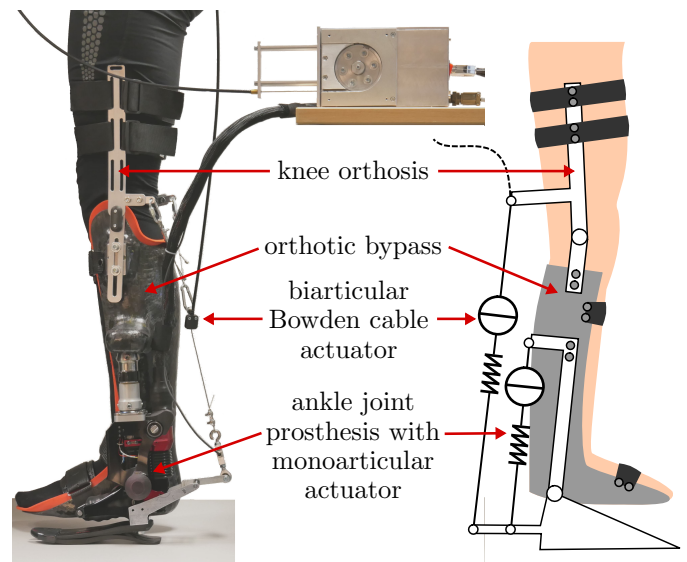


Fig. 1. Hardware setup and schematic representation with monoarticular ankle joint prosthesis, biarticular Bowden cable actuator, knee orthosis, and orthotic bypass system. Offboard placed power supply, motion controllers, real time target computer, foot cosmetic and sports shoe are not shown.

2. HARDWARE

The hardware setup shown in Fig. 1 consists of an active ankle joint prosthesis, an offboard Bowden cable actuator, a knee orthosis, and an orthotic bypass to enable persons without TTA to test the system. The power supply, the motor drives and the real-time target computer are placed offboard. An xPC-Target prototyping platform with a sampling frequency of 1 kHz is used to control the system.

2.1 Ankle Joint Prosthesis

The prosthesis in use is a lab version of the Ruggedized Odysseus Ankle prosthesis (SpringActive), an updated version of the WRA. It comprises a 200 W brushless DC (BLDC) motor (maxon *EC-4pole 30*), a 2.44:1 pulley, a 1 mm pitch ball screw and a lever mechanism to actuate a serial steel spring. A Pacifica LP carbon foot (stiffness category 9), a foot cosmetic and a sports shoe are used. Encoders measure motor position and ankle joint angle, by which the deflection of the serial spring and the resulting ankle torque can be estimated. A 6-axis inertial measurement unit is placed in the shank of the prosthesis. Motor and sensors are connected to the offboard placed motor drive and real-time target by cable.

2.2 Bowden Cable Actuator

The Bowden cable actuator consists of a 180 W BLDC motor (maxon *EC-i 52*), a 19:1 planetary gear and a disc (35 mm radius) coiling a 1.5 mm steel cable. The length of the Bowden cable is 2 m, allowing enough RoM to walk on a treadmill. A force sensor is used to measure the force at the end of the Bowden cable.

2.3 Knee Orthosis and Bypass System

A knee orthosis comprising a simple rotational link is attached to a custom orthotic bypass. The prosthesis is linked in parallel to the bypass. As the leg length of the prosthesis side increases by approximately 5 cm, the shoe of the contra lateral leg is equipped with an additional sole to minimize the length difference. Rigid belts are used at the front side of the thigh to transfer knee bending forces into the human tissue. Elastic belts are used on the backside of the thigh to ensure comfortable fit. Due to the design the bypass can also be replaced by a modified prosthesis socket to test the biarticular prosthesis with persons with TTA.

The orthotic bypass prevents the user from moving its ankle. The actuation of the knee joint through the gastrocnemius muscle is still possible in the given setup. This is negligible for the verification, whether the given setup can generate desired forces in the Bowden cable. When used by a person with TTA, the remaining of the gastrocnemius muscle of the user cannot affect the knee.

The lever arm ratio between knee and ankle joint is selected to match the human gastrocnemius muscle lever arm ratio. The gastrocnemius lever arms at the knee and the ankle joint are taken from literature. Ratios $\frac{r_{\text{ankle}}}{r_{\text{knee}}}$ vary between $\frac{5.3 \text{ cm}}{2.5 \text{ cm}} = 2.12$ (McLean et al. (2003)) and $\frac{3.45 \text{ cm}}{1.35 \text{ cm}} = 2.56$ (Van der Burg et al. (2005)). The ratio is chosen to be $\frac{r_{\text{ankle}}}{r_{\text{knee}}} = \frac{15 \text{ cm}}{6 \text{ cm}} = 2.5$.

3. MODELING AND IDENTIFICATION

The ankle joint prosthesis and the Bowden cable actuator can both be seen as SEAs and can therefore be modeled in a similar way. The prosthesis has a specified elasticity in form of a linear steel spring, whereas the Bowden cable actuator's stiffness is composed of the stiffness of cable and interfering human tissue. For the ankle joint prosthesis, the load position is known from ankle angle measurement, whereas for the Bowden cable actuator it is unknown. The ankle joint prosthesis has limited RoM due to mechanical stops, whereas the Bowden cable actuator can easily be detached to move freely. In this section we will model both actuators and demonstrate the identification of the system parameters.

Motor drives of both systems are operated in current control mode. Current loop time constants are small enough, therefore current dynamics can be neglected.

3.1 Ankle Joint Prosthesis

The ankle joint prosthesis is modeled as a SEA with an inertia J_P and an ideal rotational spring k_P . The lever kinematic can be linearized as a gear ratio q_P . Friction is modeled as Coulomb friction $M_{C,P}$ and viscous damping d_P . With the motor angle φ_P , the motor torque constant c_P and the motor current i_P equation of motion of the ankle joint prosthesis becomes

$$J_P \ddot{\varphi}_P = c_P i_P - d_P \dot{\varphi}_P - M_{C,P}(\dot{\varphi}_P) - q_P M_P \quad (1)$$

with

$$M_P = k_P (q_P \varphi_P - \Delta\alpha) . \quad (2)$$

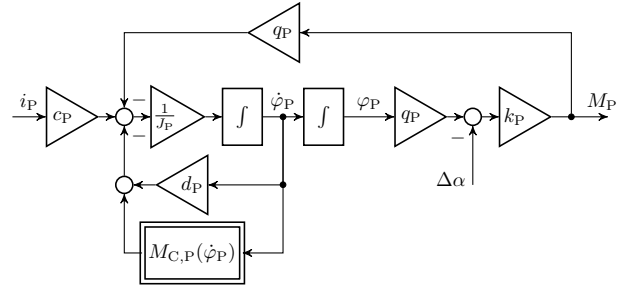


Fig. 2. Block diagram of the ankle joint prosthesis

The block diagram of the system is shown in Fig. 2. The identification of the model parameters is conducted as follows.

The gear ratio q_P , the motor constant c_P and the stiffness k_P are determined from CAD data and datasheets. The remaining parameters J_P , d_P , and $M_{C,P}$ are estimated from current step responses with the prosthesis being able to move freely, hence $M_P = 0$. Assuming $M_{C,P}(\dot{\varphi}_P) = M_{C,P}$ to be constant the step response of the motor velocity $\dot{\varphi}_P(t)$ from (1) for $i_P(t) = I\sigma(t)$ becomes

$$\dot{\varphi}_P(t) = \dot{\varphi}_{P,0} e^{-\frac{d_P}{J_P} t} + \frac{c_P I - M_{C,P}}{d_P} \left(1 - e^{-\frac{d_P}{J_P} t} \right), t \geq 0 . \quad (3)$$

With measured $\tilde{\varphi}_P$ and estimated $\hat{\varphi}_P$ the parameters $\theta = [J_P, d_P, M_{C,P}]$ are estimated from output error minimization. $M_{C,P}$ and d_P mainly influence steady state, whereas $\frac{d_P}{J_P}$ defines transient behavior. Therefore, the output error is minimized over $n > 2$ different step heights I_k resulting in

$$\theta = \arg \min_{\theta} \sum_{k=1}^n \int_0^{t_{\text{end},k}} \left(\tilde{\varphi}_{P,k}(t) - \hat{\varphi}_{P,k}(t, I_k, \theta) \right) . \quad (4)$$

Fig. 3 shows measured and estimated motor velocity for $n = 3$.

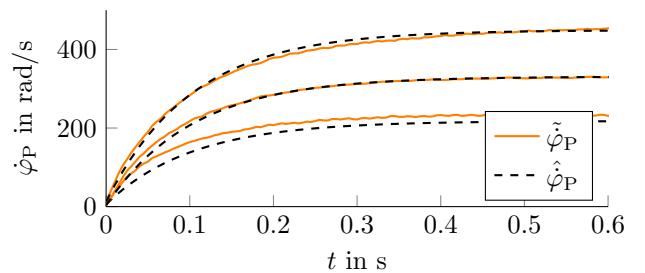


Fig. 3. Step responses of the ankle joint prosthesis motor angular velocity $\dot{\varphi}_P$ for multiple input current step heights and fits by an output error minimization

3.2 Bowden Cable Actuator

The Bowden cable actuator's equation of motion is defined similar to (1) as

$$J_B \ddot{\varphi}_B = c_B i_B - d_B \dot{\varphi}_B - M_{C,B}(\dot{\varphi}_B) - q_B F_B \quad (5)$$

with the nonlinear Bowden cable force F_B being a function of actuator and load position $\Delta x_B = q_B \varphi_B - x_L$

$$F_B = f(\Delta x_B) . \quad (6)$$

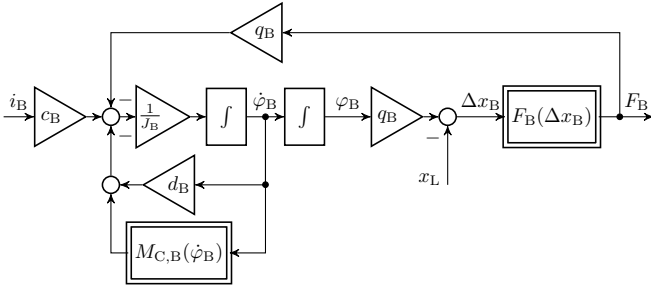


Fig. 4. Block diagram of the Bowden cable actuator

The corresponding block diagram is shown in Fig. 4. The parameters J_B , c_B and q_B are determined from CAD data and datasheets. $M_{C,B}$ and d_B can be determined similar to $M_{C,P}$ and d_P in the previous section. The actuator stiffness is estimated as follows.

The stiffness of the Bowden cable actuator is composed of the stiffness of the cable, the carbon foot and the interfering human tissue at the thigh belts. To identify the stiffness parameters, a conservatively tuned cascade controller (outer P force cascade, inner PI velocity cascade) is designed. Triangular-shaped reference forces are commanded to the actuator, while Bowden cable deflection is measured. The ankle joint prosthesis is commanded to produce zero ankle torque. Multiple repetitions are performed while standing with a straight leg (knee angle $\alpha_{\text{knee}} = 180^\circ$) and a bent leg condition ($\alpha_{\text{knee}} = 140^\circ$). The results are shown in Fig. 5. Loading curves look equal for straight and bent leg condition, hence the influence of the knee angle can be neglected.

A quadratic spring

$$F_B = a(\Delta x_B)^2 + b\Delta x_B \quad (7)$$

is fitted to the measurements, where F_B is the measured force and Δx_B is the Bowden cable deflection. The lin-

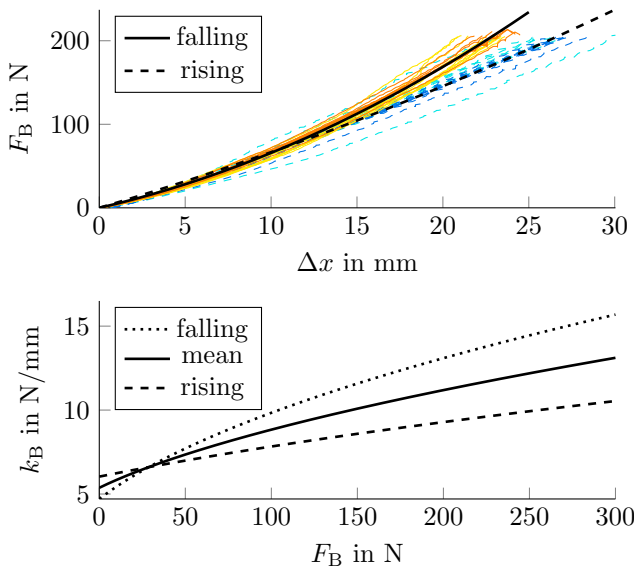


Fig. 5. Top plot: measured rising (cyan: straight-leg, blue: bent-leg) and falling (yellow: straight-leg, orange: bent-leg) forces F_B and fitted quadratic spring. Bottom plot: linearized Bowden cable actuator stiffness k_B .

earized Bowden cable stiffness is

$$k_B = \left. \frac{dF_B}{d\Delta x_B} \right|_{\Delta x_{B,0}} = 2a\Delta x_{B,0} + b, \quad (8)$$

where $F_{B,0}$ and $\Delta x_{B,0}$ denote cable force and deflection at a stationary working point. With

$$\Delta x_{B,0} = \frac{-b}{2a} + \sqrt{\frac{b^2}{4a^2} + \frac{F_{B,0}}{a}} \quad (9)$$

k_B can be expressed as function of the cable force $F_{B,0}$ as

$$k_B = \sqrt{b^2 + 4aF_{B,0}}. \quad (10)$$

Averaged parameters for rising and falling forces are $a = 124\,000 \frac{\text{N}}{\text{m}^2}$ and $b = 5\,400 \frac{\text{N}}{\text{m}}$.

4. CONTROL

As both actuators can be modeled as series elastic actuators with measured output torque (or force) and load position as disturbance input, identical control structures will be used for both systems. For better reading, gear ratios q_* are omitted. System parameters are denoted c , J , d and k with input current i , motor position φ , disturbance φ_L and output M as shown in Fig. 6. Coulomb friction is neglected.

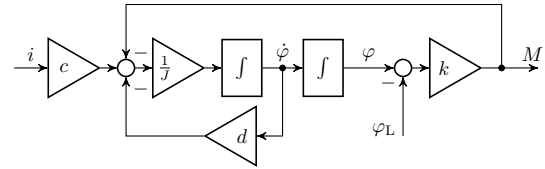


Fig. 6. Block diagram of general series elastic actuator

Time derivation of M leads to

$$\dot{M} = k(\dot{\varphi} - \dot{\varphi}_L). \quad (11)$$

The actuator equation of motion can be formulated as

$$\ddot{\varphi} = \frac{1}{J}(ci - d\dot{\varphi} - M). \quad (12)$$

Equations (11) and (12) lead to the state space representation

$$\begin{bmatrix} \dot{M} \\ \dot{\varphi} \end{bmatrix} = \underbrace{\begin{bmatrix} 0 & k \\ -\frac{1}{J} & -\frac{d}{J} \end{bmatrix}}_{\mathbf{A}} \underbrace{\begin{bmatrix} M \\ \varphi \end{bmatrix}}_{\mathbf{x}} + \underbrace{\begin{bmatrix} 0 \\ \frac{c}{J} \end{bmatrix}}_{\mathbf{b}} i + \begin{bmatrix} -k \\ 0 \end{bmatrix} \dot{\varphi}_L, \quad (13)$$

$$M = \underbrace{\begin{bmatrix} 1 & 0 \end{bmatrix}}_{\mathbf{c}^T} \mathbf{x}.$$

This state space representation allows the design of a controller that utilizes measured torque and motor velocity using state space methods.

The suggested control structure is based on Roppenecker (2009) and consists of a model-based feedforward control and a PI-control with state feedback as shown in Fig. 7. The feedforward control is designed to achieve good command action and disturbance rejection towards measurable disturbances, whereas the PI-control with state feedback handles modeling errors, unmeasured disturbances and guarantees zero tracking error at steady state. The design of both controllers will be described in the following sections.

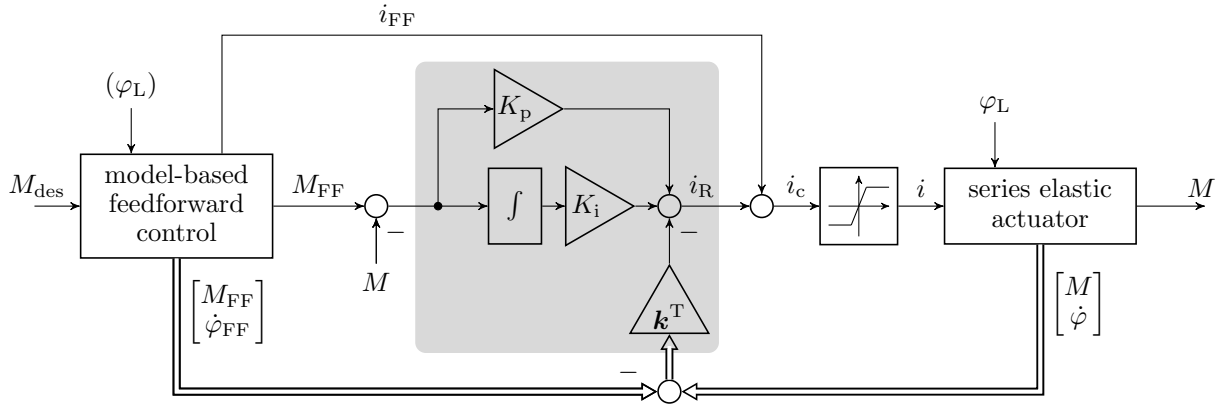


Fig. 7. Control structure with model-based feedforward control, PI-control with state feedback (grey area), current saturation and series elastic actuator. An integrator anti-windup is implemented, but not shown for reasons of simplicity. Parentheses at the load angle φ_L indicate, that φ_L is only fed into the feedforward control, if it is measurable.

4.1 Model-Based Feedforward Control

The model-based feedforward control consists of a controlled actuator model. It can be seen as a prefilter, which generates a modified reference and an corresponding control input, that suit the closed loop dynamics of the feedforward model. The inputs of the model-based feedforward control are the desired torque M_{des} and, if available, the disturbance input φ_L . The outputs are the modified reference M_{FF} and the modified state vector $\mathbf{x}_{FF} = [M_{FF} \ \dot{\varphi}_{FF}]^T$ as well as the feedforward control input i_{FF} .

For the system (13) a linear state feedback controller with constant prefilter

$$i_{FF} = fM_{des} + \mathbf{k}_{FF}^T \mathbf{x}_{FF} \quad (14)$$

will lead to zero steady state error, good command action and disturbance rejection.

In general high torques are required and actuator saturation can occur during prosthesis operation. Therefore, instead of (14), the following control law

$$i_{FF} = \begin{cases} i_{FF,sat} & , fM_{des} + \mathbf{k}_{FF}^T \mathbf{x}_{FF} > i_{FF,sat} \\ -i_{FF,sat} & , fM_{des} + \mathbf{k}_{FF}^T \mathbf{x}_{FF} < -i_{FF,sat} \\ fM_{des} + \mathbf{k}_{FF}^T \mathbf{x}_{FF} & , \text{otherwise} \end{cases} \quad (15)$$

is used, where $i_{FF,sat}$ is the saturation current allocated to the feedforward control. It is chosen to be 75% of the maximum current available.

State space representation (13) is used to design the state feedback \mathbf{k}_{FF}^T from (14) as a linear-quadratic regulator with weight matrices \mathbf{Q} and R for the states and the input. The parameter f is chosen such that the steady state error is zero. The resulting controller is then implemented as stated in (15).

The implementation of the feedforward model with (13) is not favorable, as it requires the time derivation of the measured disturbance φ_L as an input. Therefore, an alternative representation of the actuator model is chosen for the implementation of the feedforward model. It is obtained by substituting $M = k(\varphi - \varphi_L)$ into (12):

$$\begin{aligned} \begin{bmatrix} \dot{\varphi} \\ \ddot{\varphi} \end{bmatrix} &= \begin{bmatrix} 0 & 1 \\ -\frac{k}{J} & -\frac{d}{J} \end{bmatrix} \begin{bmatrix} \varphi \\ \dot{\varphi} \end{bmatrix} + \begin{bmatrix} 0 \\ \frac{c}{J} \end{bmatrix} i + \begin{bmatrix} 0 \\ \frac{k}{J} \end{bmatrix} \varphi_L, \quad (16) \\ M &= [k \ 0] \begin{bmatrix} \varphi \\ \dot{\varphi} \end{bmatrix} - k\varphi_L. \end{aligned}$$

For the ankle joint prosthesis, the disturbance φ_L is measurable. For the Bowden cable actuator, the disturbance x_L results from the knee and the ankle motion, where only the latter is measurable. Therefore, x_L is not feed into the feedforward control and has to be handled by the feedback controller.

4.2 PI-Control with State Feedback

Ignoring the saturation block in Fig. 7 the dynamics of PI-control with state feedback and series elastic actuator can be derived by adding the integrator state

$$\dot{x}_I = M_{FF} - M \quad (17)$$

and the control gains K_i , K_p and \mathbf{k}_e^T to system (13) resulting in

$$\begin{bmatrix} \dot{M} \\ \dot{\varphi} \\ \dot{x}_I \end{bmatrix} = \underbrace{\begin{bmatrix} 0 & k & 0 \\ -\frac{1}{J} & -\frac{d}{J} & 0 \\ -1 & 0 & 0 \end{bmatrix}}_{\mathbf{A}_e} \underbrace{\begin{bmatrix} M \\ \varphi \\ x_I \end{bmatrix}}_{\mathbf{x}_e} + \underbrace{\begin{bmatrix} 0 \\ \frac{c}{J} \\ 0 \end{bmatrix}}_{\mathbf{b}_e} i + \begin{bmatrix} -k \\ 0 \\ 0 \end{bmatrix} \varphi_L + \begin{bmatrix} 0 \\ 0 \\ 1 \end{bmatrix} M_{FF}, \quad (18)$$

$$i_R = \underbrace{[-\mathbf{k}_e^T - [K_p \ 0] \quad K_i]}_{\mathbf{k}_e^T} \mathbf{x}_e + K_p M_{FF}. \quad (19)$$

The state feedback \mathbf{k}_e^T is designed as linear-quadratic regulator for the system matrices \mathbf{A}_e and \mathbf{b}_e with weight matrices \mathbf{Q}_e and R_e . The proportional gain is chosen according to

$$K_p = -(\mathbf{c}^T \mathbf{A}^{-1} \mathbf{b})^{-1} \quad (20)$$

as suggested in Föllinger et al. (1994). The control gains \mathbf{k}_e^T and K_i are then chosen to satisfy

$$\mathbf{k}_e^T = [-\mathbf{k}^T - [K_p \ 0], \quad K_i] \quad (21)$$

from (19). An anti-windup feeding back the difference between control input $i_c = i_{FF} + i_R$ and actual current i (see Fig. 7) onto the integrator input

$$e_{aw} = \frac{i - i_c}{T_{aw}K_i} \quad (22)$$

with $T_{aw} = 0.01$ is used to prevent integrator windup.

4.3 Controller Tuning

For the tuning of model-based feedforward control and PI-control with state feedback the weight matrices \mathbf{Q} and \mathbf{R} as well as \mathbf{Q}_e and \mathbf{R}_e have to be specified. Suitable values require some experiments but can be determined intuitively from either looking at step responses or eigenvalues of the closed loop system. \mathbf{Q} and \mathbf{Q}_e are chosen as diagonal matrices $\mathbf{Q} = \text{diag}(q_{11}, q_{22})$ and $\mathbf{Q}_e = \text{diag}(q_{e,11}, q_{e,22}, q_{e,33})$. The elements q_{11} , $q_{e,11}$ and $q_{e,33}$ are chosen high to lead to a desired bandwidth, q_{22} and $q_{e,22}$ are raised from zero to guarantee proper damping.

For the Bowden cable actuator's controller, a linearized stiffness $k_B(F_0)$ has to be specified for the controller design and the implementation of the feedforward model. We chose $F_0 = 100$ N, which is a typical force to be expected during experiments. For both systems, ankle joint prosthesis and Bowden cable actuator, the model-based feedforward control and the PI-control with state feedback are designed to have a bandwidth of 8 Hz and 2.5 Hz, respectively.

5. EVALUATION

The biarticular prosthesis is evaluated in a simple walking experiment on a treadmill with constant velocity. Therefore, a time based control approach generating reference torques based on discrete events is suitable. The purpose of the experiment is to demonstrate, that the given hardware setup and the proposed control structure can track the desired ankle torques with a variable distribution between the two actuators.

5.1 Reference Torque Generation

A gait phase variable t_g is used to estimate the users progression within the stride. The gait phase $t_g \in [0, 1]$ is estimated based on the latest prosthesis touchdown $t_{TD,i}$ and the duration of the previous prosthesis stride $T_{prev} = t_{TD,i} - t_{TD,i-1}$ according to

$$t_g = \begin{cases} \frac{t - t_{TD,i}}{T_{prev}} & , t - t_{TD,i} \leq T_{prev} \\ 1 & , \text{otherwise} \end{cases} \quad (23)$$

where $t_{TD,i-1}$ denotes the touchdown prior to the latest touchdown. Touchdowns are detected based on positive zero crossings of the shank angular velocity, which occur at the end of the swing phase for various walking speeds (Grimmer et al. (2019)).

Ankle reference torques $M_{ref}(t_g)$ are generated based on the human ankle torques $M_{A,H}(t_g)$ and angles $\alpha_{A,H}(t_g)$ from Lipfert (2010) as well as the gait phase t_g and the prosthesis ankle angle $\alpha(t)$ as

$$M_{ref}(t_g) = -k_A(\alpha(t) - \alpha_{A,H}(t_g)) + M_{A,H}(t_g). \quad (24)$$

Here k_A denotes the prosthesis ankle stiffness, which modifies the reference torque when deviating from normative ankle angle trajectories $\alpha_{A,H}(t_g)$. In general, k_A is

normalized to the users body mass m_{user} . Experiments on unimpaired human subjects show that human ankle impedance is mainly elastic when being disturbed during the stance phase with normalized stiffness values between 1.5 to 6.5 $\frac{\text{Nm}}{\text{rad kg}}$ (Rouse et al. (2014)). In our experiments, we specified $k_A = m_{user} 4 \frac{\text{Nm}}{\text{rad kg}}$.

Plantar flexing torques are counted positive. Therefore, the human gastrocnemius muscle can only generate positive ankle torques. The reference ankle torque is allocated to the ankle joint prosthesis and the Bowden cable actuator according to

$$M_{P,des} = (1 - \kappa) M_{ref} H(M_{ref}) + M_{ref} H(-M_{ref}) \quad (25)$$

$$F_{B,des} = \kappa \frac{M_{ref}}{r_{ankle}} H(M_{ref}) \quad (26)$$

where $H(\cdot)$ is the Heaviside function and κ is a free parameter to set the distribution of ankle torque between the two actuators.

5.2 Walking Experiment

A walking experiment was performed with a subject (1.90 m, 85 kg) walking on a treadmill at a constant velocity of 1.0 m/s. The study protocol was approved by the institutional review board of TU Darmstadt.

The parameter κ was chosen constant for multiple strides in order to familiarize the subject to the assistance. Values varied between 0.1 and 0.4. The ankle torque and ankle angle are estimated from the sensors of the ankle joint prosthesis and the Bowden cable actuator. The resulting ankle torque M_{ankle} is the sum of the ankle torque of the ankle joint prosthesis M_P and the Bowden cable actuator M_B

$$M_{ankle} = M_P + \underbrace{r_{ankle} F_B}_{M_B} \quad (27)$$

and the resulting knee torque is

$$M_{knee} = r_{knee} F_B. \quad (28)$$

6. EXPERIMENTAL RESULTS AND DISCUSSION

We showed that despite the differences between the ankle joint prosthesis and the Bowden cable actuator, both systems can be modeled similarly as series elastic actuators. Methods to identify the system parameters are demonstrated exemplary for both actuators. A torque controller consisting of a model-based feedforward control and a PI-control with state feedback is designed for each of the actuators. A method to generate reference torques based on healthy human ankle biomechanics and a gait phase variable is introduced.

Based on this a walking experiment could be conducted to evaluate the biarticular transtibial prosthesis and the designed controllers. Fig. 8 shows a typical stride for $\kappa = 0.3$. The tracking performance for other strides and values of κ between 0.1 and 0.4 is comparable to the results shown in Fig. 8. Beside the torque and the angle of the ankle joint prosthesis and the torque generated by the Bowden cable actuator, the human ankle angle $\alpha_{A,H}(t_g)$ and torque $M_{A,H}(t_g)$ used in (24) are shown.

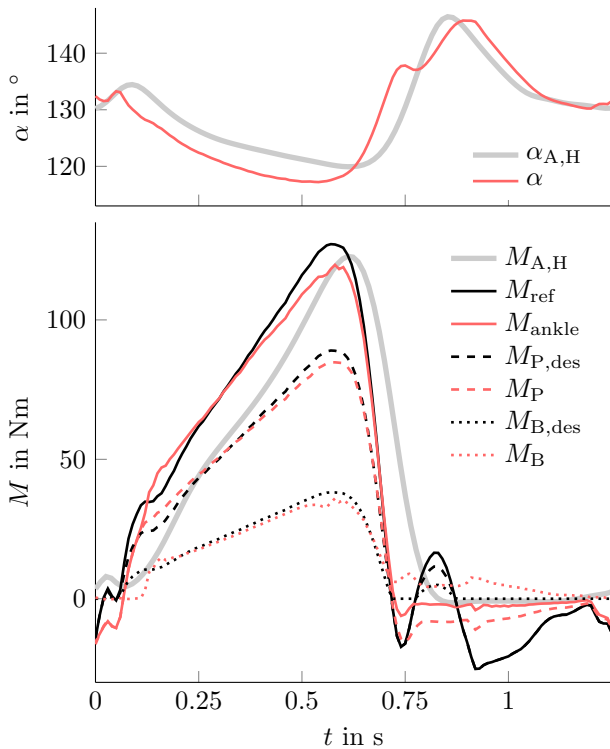


Fig. 8. Exemplary results of one stride. Top plot: prosthesis ankle angle α . Bottom plot: overall desired and measured ankle torque M and contributions of ankle joint prosthesis and Bowden cable actuator for $\kappa = 0.3$. Human ankle angle $\alpha_{A,H}$ and torque $M_{A,H}$ from Lipfert (2010) scaled to the duration of the stride are shown in light gray.

The principal shape of the ankle angle α and the ankle torque M_{ankle} matches those of $\alpha_{A,H}$ and $M_{A,H}$. The stance phase lasts until $t \approx 0.75$ s, followed by the swing phase. The results show that the reference torque generated from (24) leads to the typical torque ramp during the stance phase. During the swing phase, the ankle torque M_{ankle} is zero and the commanded torque M_{ref} leads to an ankle angle α similar to $\alpha_{A,H}$. The shorter stance phase compared to the human ankle trajectories $\alpha_{A,H}$ and $M_{A,H}$ could be caused by the additional weight of the prosthesis and the bypass. The smaller ankle angle α compared to $\alpha_{A,H}$ during the stance phase results from the individual loading of the prosthesis by the user. This leads, according to (24), to an increased ankle torque reference $M_{\text{ref}}(t_g)$ of $-k_A(\alpha(t) - \alpha_{A,H}(t_g))$ compared to $M_{A,H}(t_g)$.

The ankle joint prosthesis has small tracking errors during the stance phase. The Bowden cable actuator has large tracking errors at early stance phase. These are caused by a slack of the Bowden cable, which results from fast ankle joint prosthesis dorsiflexion at early stance phase. At phases of higher torque assistance, the Bowden cable actuator shows small tracking errors. During the swing phase the maximum knee torque generated by the Bowden cable force is lower than 4 Nm and the root mean square torque is 1.6 Nm. These values are small compared to the typical knee torque during level walking, which reaches maximum torque values of 40 Nm (Lipfert (2010)) for the given user mass and walking velocity.

In combination, both systems can generate ankle torques and ankle angles comparable to human ankle biomechanics during level walking with a scalable distribution of torque between the actuators.

7. CONCLUSION

With the given hardware setup the torque tracking results of the monoarticular ankle joint prosthesis and the biarticular Bowden cable actuator demonstrate that the given hardware setup and the proposed control structure is capable of precisely generating the desired torques and forces. Our future work will focus on determining suitable reference torques and distribution to the actuators to improve the gait patterns of persons with TTA with respect to gait symmetry and metabolic cost. Potential approaches will be the systematic variation of parameters such as the support level and the support timing of the biarticular actuator as well as human in the loop optimizations.

REFERENCES

- Eilenberg, M.F., Kuan, J.Y., and Herr, H. (2018). Development and evaluation of a powered artificial gastrocnemius for transtibial amputee gait. *Journal of Robotics*.
- Endo, K., Swart, E., and Herr, H. (2009). An artificial gastrocnemius for a transtibial prosthesis. In *2009 Annual International Conference of the IEEE Engineering in Medicine and Biology Society*, 5034–5037. IEEE.
- Ferris, A.E., Aldridge, J.M., Rábago, C.A., and Wilken, J.M. (2012). Evaluation of a powered ankle-foot prosthetic system during walking. *Archives of physical medicine and rehabilitation*, 93(11), 1911–1918.
- Föllinger, O., Dörrscheidt, F., and Klittich, M. (1994). Regelungstechnik - Einführung in die Methoden und ihre Anwendung. *Hüthig Buch Verlag Heidelberg*, 8. überarb. Aufl.
- Grimmer, M., Holgate, M., Ward, J., Boehler, A., and Seyfarth, A. (2017). Feasibility study of transtibial amputee walking using a powered prosthetic foot. In *2017 International Conference on Rehabilitation Robotics (ICORR)*, 1118–1123. IEEE.
- Grimmer, M., Schmidt, K., et al. (2019). Stance and swing detection based on the angular velocity of lower limb segments during walking. *Frontiers in neurorobotics*, 13, 57.
- Grimmer, M. and Seyfarth, A. (2014). Mimicking human-like leg function in prosthetic limbs. In *Neuro-Robotics*, 105–155. Springer.
- Grün, M., Müller, R., and Konigorski, U. (2012). Model based control of series elastic actuators. In *4th IEEE RAS/EMBS International Conference on Biomedical Robotics and Biomechanics (Biorob)*, 538–543. IEEE.
- Herr, H. and Grabowski, A.M. (2011). Bionic ankle-foot prosthesis normalizes walking gait for persons with leg amputation. *Proceedings of the Royal Society B: Biological Sciences*, 279(1728), 457–464.
- Kong, K., Bae, J., and Tomizuka, M. (2009). Control of rotary series elastic actuator for ideal force-mode actuation in human-robot interaction applications. *IEEE/ASME transactions on mechatronics*, 14(1), 105–118.
- Lipfert, S.W. (2010). *Kinematic and dynamic similarities between walking and running*. Kovač Hamburg.

- McLean, S.G., Su, A., and van den Bogert, A.J. (2003). Development and validation of a 3-d model to predict knee joint loading during dynamic movement. *Journal of biomechanical engineering*, 125(6), 864–874.
- Pratt, G.A. and Williamson, M.M. (1995). Series elastic actuators. In *Proceedings 1995 IEEE/RSJ International Conference on Intelligent Robots and Systems. Human Robot Interaction and Cooperative Robots*, volume 1, 399–406. IEEE.
- Quinlivan, B., Lee, S., et al. (2017). Assistance magnitude versus metabolic cost reductions for a tethered multiarticular soft exosuit. *Science Robotics*, 2(2), 4416.
- Roppenecker, G. (2009). Zustandsregelung linearer Systeme - Eine Neubetrachtung (state feedback control of linear systems - a renewed approach). *at-Automatisierungstechnik Methoden und Anwendungen der Steuerungs-, Regelungs- und Informationstechnik*, 57(10), 491–498.
- Rouse, E.J., Hargrove, L.J., Perreault, E.J., and Kuiken, T.A. (2014). Estimation of human ankle impedance during the stance phase of walking. *IEEE Transactions on Neural Systems and Rehabilitation Engineering*, 22(4), 870–878.
- Schumacher, C., Sharbafi, M., Seyfarth, A., and Rode, C. (2020). Biarticular muscles in light of template models, experiments and robotics: a review. *Journal of the Royal Society Interface*, 17(163), 20180413.
- Vallery, H., Ekkelenkamp, R., Van Der Kooij, H., and Buss, M. (2007). Passive and accurate torque control of series elastic actuators. In *2007 IEEE/RSJ international conference on intelligent robots and systems*, 3534–3538. IEEE.
- Van der Burg, J., Casius, L., et al. (2005). Factors underlying the perturbation resistance of the trunk in the first part of a lifting movement. *Biological cybernetics*, 93(1), 54–62.
- Willson, A.M., Richburg, C.A., Czerniecki, J., Steele, K.M., and Aubin, P.M. (2020). Design and development of a quasi-passive transtibial biarticular prosthesis to replicate gastrocnemius function in walking. *Journal of Medical Devices*, 14(2).
- Witte, K.A., Zhang, J., Jackson, R.W., and Collins, S.H. (2015). Design of two lightweight, high-bandwidth torque-controlled ankle exoskeletons. In *2015 IEEE International Conference on Robotics and Automation (ICRA)*, 1223–1228. IEEE.